Unified Landau description of the tetragonal, orthorhombic, and monoclinic phases of zirconia

Giuseppe Fadda,[1,*] Lev Truskinovsky,[2,†] and Giovanni Zanzotto[1,‡]

[1]*Dipartimento di Metodi e Modelli Matematici per le Scienze Applicate (DMMMSA), Università di Padova, Via Belzoni 7, 35131 Padova, Italy*

[2]*Department of Aerospace Engineering and Mechanics, University of Minnesota, 110 Union Street SE, Minneapolis, Minnesota 55455*

We compute an explicit lowest-order polynomial form of the strain-dependent Gibbs potential which provides a unified description of the tetragonal, orthorhombic, and monoclinic phases of zirconia (ZrO_2). The resulting energy function interpolates well the available experimental data for this material, reproducing its known elastic moduli, equilibrium strains, and phase diagram to about 1700 K and 8 GPa.

I. INTRODUCTION

Zirconia (ZrO_2), being the most important toughening agent for ceramics, is a widely investigated material interesting from both the theoretical and experimental points of view.[1] In this paper we derive an energy function which depends on the temperature and strain tensor,[2] and allows for a unified quantitative description of the mechanical and thermal properties of zirconia in the range of temperatures and pressures where a tetragonal-orthorhombic-monoclinic (t-o-m) triple point is observed, see Fig. 1. In order to write a free-energy function suitable for ZrO_2, we extend the approach initiated in Refs. 9 and 10, and that was developed in a recent paper[11] where the strain energy of generic three-phase elastic crystals exhibiting a t-o-m triple point was investigated. To match the available experimental data on ZrO_2, four new coupling terms were added to the polynomial proposed in Ref. 11. This resulted in a more complex bifurcation diagram, with the appearance of a second orthorhombic phase, see Fig. 5 below. In spite of its relative simplicity, the present model reproduces remarkably well not only the phase diagram of t-o-m ZrO_2 and the experimental tetragonal and monoclinic lattice parameters, but also the known elastic moduli of the monoclinic phase and the bulk modulus of the orthorhombic phase. The final strain energy function can be used directly in the studies of zirconia crystals under general nonhydrostatic loads, including an improved modeling of transformation toughening.[12–14]

This paper is organized as follows. In Sec. II we discuss the crystallographic aspects of the model and, based on available data which include the reported orientation relationships, establish the transformation mechanism for the t-o-m zirconia polymorphs. In particular, we suggest for the well-known tetragonal-monoclinic transformation in ZrO_2 a mechanism that is different from the one usually considered in the literature.[3,13,15] In Sec. III we develop a unified Landau description for t-o-m zirconia, and construct the minimal polynomial expansion of the energy allowing for an accurate fitting and reproduction of the experimental data. In Sec. IV we compare the results from the model with data on the spontaneous strains, elastic moduli, and phase diagram of zirconia. Concluding remarks are made in Sec. V; a brief description of the fitting procedure for the Landau coefficients is given in the Appendix.

II. TRANSFORMATION MECHANISM OF t-o-m ZIRCONIA

Zirconia exhibits tetragonal (t), orthorhombic "orthoI" (o), and monoclinic (m) phases, with a triple point as in Fig. 1. References 16–23 give detailed crystallographic descriptions of these and other zirconia polymorphs, and present the experimental phase diagrams.[24]

We begin with the observation that the lattice structures of t-o-m ZrO_2 can all be described as originating from small deformations of a primitive tetragonal Bravais lattice ("skeleton"), spanned by three mutually orthogonal basis vectors t_1, t_2, and t_3. The skeleton is constituted by the *corner* Zr atoms of the so-called "face-centered tetragonal cell" of zirconia, which in turn is a slight distortion of the conventional fcc cell of the cubic ZrO_2 structure (see Fig. 2).[25] As we consider only the skeletal deformations and disregard the atoms inside the cell, only the point groups are relevant for the description of the invariance properties of the model. The point group $\mathcal{T}_3$ of the tetragonal lattice in Fig. 2 is the following:

$$\mathcal{T}_3 = \{1, R_{t_1}^{\pi}, R_{t_2}^{\pi}, R_{t_3}^{\pi}, R_{t_1+t_2}^{\pi}, R_{t_1-t_2}^{\pi}, R_{t_3}^{\pi/2}, R_{t_3}^{3\pi/2}\}, \quad (1)$$

where R_k^{ψ} denotes a rotation of angle ψ about the axis k. In Eq. (1) and hereafter, we only list the elements of point groups which have a positive determinant.

We must now identify the deformations that produce the skeletal lattices of the orthoI and monoclinic phases, when
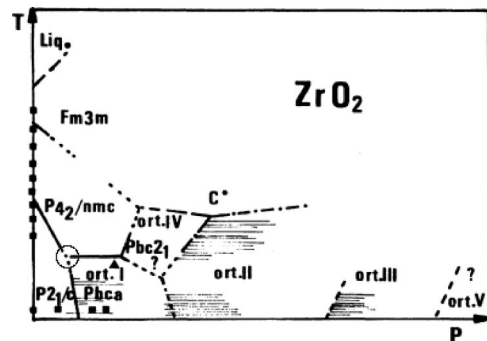

FIG. 1. Phase diagram of ZrO_2, from Ref. 20. The t-o-m triple point considered in this paper, marked by a circle in the figure, is near 840 K and 1.8 GPa.
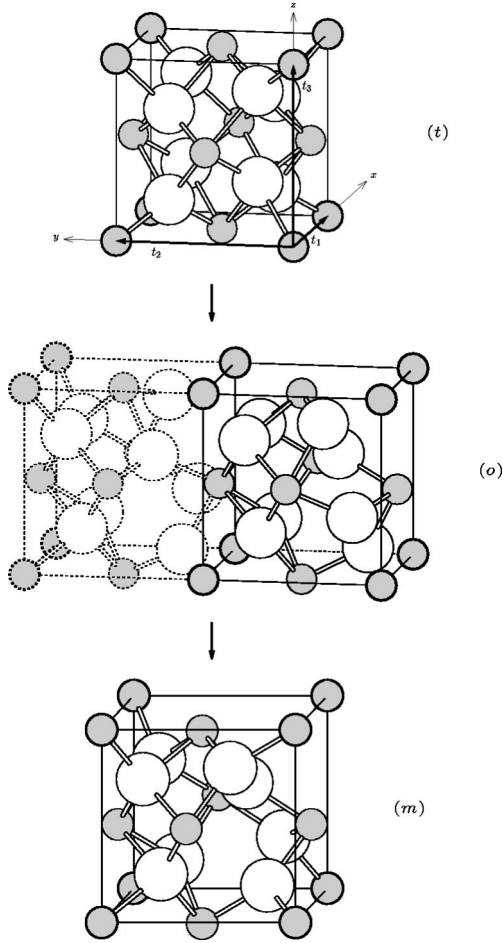
FIG. 2. Crystallography of the t-o-m phases of ZrO_2 (Zr atoms are in gray, O atoms in white). The Zr skeletal lattice, whose strain is considered in this theory, is marked in bold; the atoms inside the skeletal cells are disregarded in this model. The orthorhombic o and monoclinic m skeletal lattices are small deformations of the primitive tetragonal reference skeleton t, spanned by the basis vectors t_a, $a=1$, 2, and 3, with the fourfold axis along t_3. The cell of orthoI ZrO_2 is constituted by two skeletal Zr cells; one of these is dashed for clarity.

applied to the reference skeleton in Fig. 2. All the kinematically distinct possibilities for lowering the symmetry of a lattice from tetragonal, to orthorhombic, down to monoclinic, or directly from tetragonal to monoclinic, have been examined in Refs. 11 and 26. By using this systematic approach, in which no transition path was *a priori* disregarded, we analyzed the experimental crystallographic data and the orientation relationships reported for the t-o-m zirconia polymorphs. The conclusions are as follows:

(i) Reference 1 reports the following orientation relationships between the t and o phases:

$$[100]_o \| [010]_t, \quad [010]_o \| [001]_t, \quad (2)$$

the indices being defined through the cell in Fig. 2. This, and the data on the positions of the two families of O atoms which, in the orthoI ZrO_2 lattice, have coordination 3 and 4 with the Zr atoms,[4,17,18,20,21] indicate that the orthoI phase of

ZrO_2 derives from a skeletal deformation that produces a primitive orthorhombic lattice whose point group is the subgroup

$$\mathcal{O}_{123} = \{1, R^{\pi}_{t_1}, R^{\pi}_{t_2}, R^{\pi}_{t_3}\} \quad (3)$$

of $\mathcal{T}_3$. See formula (A2) in the Appendix for the explicit expression of the related strain matrix.

(ii) The best-established orientation relationships for the t-m transformation in ZrO_2 are:[27–30]

$$(100)_m \| (010)_t, \quad [010]_m \| [001]_t. \quad (4)$$

This means that $c_t \| b_m$, i.e., the fourfold c axis of the t phase is parallel to the twofold b axis of the m phase; the point group of the m phase of ZrO_2 is therefore the following subgroup:

$$\mathcal{M}_3 = \{1, R^{\pi}_{t_3}\} \quad (5)$$

of $\mathcal{T}_3$. The corresponding strain matrix is given in formula (A4) of the Appendix. The overall symmetry-breaking mechanism for t-o-m ZrO_2 is thus the following, represented in Fig. 2:

$$\mathcal{T}_3 \rightarrow \mathcal{O}_{123} \rightarrow \mathcal{M}_3 \quad (6)$$

(the same t-o-m transformation path is also a consequence of the discussion in Ref. 1). Consequently the well-known tetragonal-monoclinic transition in this material is $\mathcal{T}_3 \rightarrow \mathcal{M}_3$. We remark that in most of the previous analyses (see, for instance, Refs. 3, 13, and 15), a different mechanism for the t-m phase change has been assumed, that is,

$$\mathcal{T}_3 \rightarrow \{\mathcal{M}_{1+2}, \mathcal{M}_{1-2}\}, \quad (7)$$

where

$$\mathcal{M}_{1+2} = \{1, R^{\pi}_{t_1+t_2}\}, \quad \mathcal{M}_{1-2} = \{1, R^{\pi}_{t_1-t_2}\} \quad (8)$$

are two other monoclinic subgroups of $\mathcal{T}_3$. The hypothesis (7) leads to a model where the t-m phase transition in ZrO_2 is driven by the bifurcation associated with the softening of the tetragonal modulus C_{44}.[31] One can see, however, that in this case there is no easy way to account for the presence of any orthorhombic structure in the phase diagram of ZrO_2. Furthermore, the best established t-m orientation relationships for zirconia do suggest a $\mathcal{T}_3 \rightarrow \mathcal{M}_3$ mechanism, as mentioned earlier. We stress that, unlike the one in Eq. (7), the path $\mathcal{T}_3 \rightarrow \mathcal{M}_3$ proposed here does not *directly* result from the softening of any tetragonal modulus. Instead, the t-m phase change in ZrO_2 is viewed as a (first-order) transformation resulting from the coexistence of "distant" energy wells with $\mathcal{T}_3$ and $\mathcal{M}_3$ symmetry (see Fig. 5 below and Ref. 11). The $\mathcal{T}_3 \rightarrow \mathcal{O}_{123}$ transition in Eq. (6), however, is driven by a bifurcation originated from the softening of the tetragonal modulus $C_{11} - C_{12}$ [see Eq. (20) below].

III. ORDER PARAMETERS AND ENERGY FUNCTION FOR t-o-m ZIRCONIA

The lattice shown in Fig. 2 corresponds to the equilibrium configuration of the t phase of ZrO_2; the variation of the lattice parameters with T is given in Refs. 35 and 36. For any deformation of this equilibrium configuration, one can assign a strain-dependent free-energy density ϕ per unit reference volume,

$$\phi = \phi(e_1, \ldots, e_6, T), \qquad (9)$$

where ϕ is a $\mathcal{T}_3$-invariant function of the strains e_I, $I = 1, \ldots, 6$. The strain components are defined and indexed as usual according to the Voigt convention

$$e_1 = e_{11}, \quad e_2 = e_{22}, \quad e_3 = e_{33},$$

$$e_4 = 2e_{23}, \quad e_5 = 2e_{13}, \quad e_6 = 2e_{12}.$$

In order to write explicitly the expansion for ϕ it is convenient to consider new strain coordinates y_I, $I = 1, \ldots, 6$, originating from the eigenspaces of the tetragonal elastic tensor [see Eq. (12) below]:

$$y_1 = e_1 + e_2 + e_3, \quad 6y_2 = e_1 + e_2 - 2e_3,$$

$$\sqrt{2}\,y_3 = e_1 - e_2, \quad y_4 = e_4, \quad y_5 = e_5, \quad y_6 = e_6. \qquad (10)$$

The strain component y_1 characterizes the homogeneous dilations; when a hydrostatic load p is applied to the crystal, its potential energy is approximated by $-py_1$. The parameter y_2 is a volume-preserving strain: together, y_1 and y_2 describe the symmetry-preserving thermal expansion of the tetragonal lattice. The activation of y_3 (i.e., y_3 becoming different from zero) breaks the equality for the lengths of the basis vectors t_1 and t_2 (see Fig. 2) while maintaining them orthogonal and thereby producing a skeletal lattice with symmetry $\mathcal{O}_{123}$ as in Eq. (3). The activation of y_6, on the other hand, breaks the orthogonality condition for t_1 and t_2 while maintaining them of the same length; if applied to an $\mathcal{O}_{123}$-orthorhombic lattice, y_6 produces a $\mathcal{M}_3$-monoclinic lattice, as required by Eq. (6).[37] The order parameters for the t-o-m transformation mechanism (6) are, therefore, the strains y_3 and y_6: $y_3 = y_6 = 0$ give the $\mathcal{T}_3$ phase; $y_3 \neq 0$ and $y_6 = 0$ give the $\mathcal{O}_{123}$ phase; y_3 and y_6, both nonzero, give the $\mathcal{M}_3$ phase (see Fig. 3).

The quadratic part ϕ_Q of the free energy ϕ is

$$\phi_Q = \frac{1}{2} C_{IJ} e_I e_J = \frac{1}{2} \bar{C}_{IJ} y_I y_J, \quad I, J = 1, \ldots, 6, \qquad (11)$$

where in the coordinates y_I the elastic tensor $\bar{C}_{IJ}$ of the tetragonal phase has the almost diagonal form

$$\bar{C}_{IJ} = \bar{C}_{JI} = \begin{pmatrix} \bar{C}_{11} & \bar{C}_{12} & & & & \\ \bar{C}_{12} & \bar{C}_{22} & & & & \\ & & C_{11} - C_{12} & & & \\ & & & C_{44} & & \\ & & & & C_{44} & \\ & & & & & C_{66} \end{pmatrix}. \qquad (12)$$

with

$$\bar{C}_{11} = \frac{1}{9}[2(C_{11} + C_{12}) + 4C_{13} + C_{33}],$$

$$\bar{C}_{12} = \frac{2}{3}[C_{11} + C_{12} - C_{13} - C_{33}],$$

$$\bar{C}_{22} = 2[C_{11} + C_{12} - 4C_{13} + 2C_{33}]. \qquad (13)$$

In these formulas, $C_{11}, C_{12}, \ldots, C_{66}$ are the six elastic moduli appearing in the standard tetragonal elastic tensor[38,39] C_{IJ} in Eq. (11). Notice that the eigenvalues associated with the eigenspaces spanned by y_3 and y_6 are $C_{11} - C_{12}$ and C_{66}, respectively.

In general, the cubic part ϕ_C of the energy ϕ is written

$$\phi_C = \frac{1}{6} C_{IJK} e_I e_J e_K = \frac{1}{6} \bar{C}_{IJK} y_I y_J y_K, \qquad (14)$$

where the coefficients C_{IJK}, for $I, J, K = 1, \ldots, 6$, are the standard third-order elastic constants of the parent tetragonal phase. Their properties can be found in Refs. 40 and 41. Among all the possible third-order terms compatible with tetragonal symmetry, we keep only the essential ones. First, we need to include $\bar{C}_{133}$, $\bar{C}_{233}$, $\bar{C}_{166}$, and $\bar{C}_{266}$, which are the coefficients of $y_1 y_3^2$, $y_2 y_3^2$, $y_1 y_6^2$, and $y_2 y_6^2$, respectively. These coupling terms allow the loads conjugate to the symmetry-preserving tetragonal strains y_1 or y_2 to activate the symmetry-breaking strains y_3 and y_6, and to produce the bifurcations required by the t-o-m phase diagram (see also Ref. 11). Furthermore, we must include the third-order terms with coefficients $\bar{C}_{344}$ and $\bar{C}_{456}$, which are necessary to complete the matrix of the monoclinic elastic moduli. No further third-order terms are considered in our model, as this does not bring obvious advantages while drastically increasing the computational difficulties of the fitting procedure.

As is shown in Ref. 11, the only terms of order higher than three necessary to generate the t-o-m triple point are the following: y_3^4, $y_3^2 y_6^2$, y_6^4, y_3^6, and y_6^6. The final expression for the Gibbs free-energy density ϕ_G of t-o-m ZrO_2 can then be written in the form
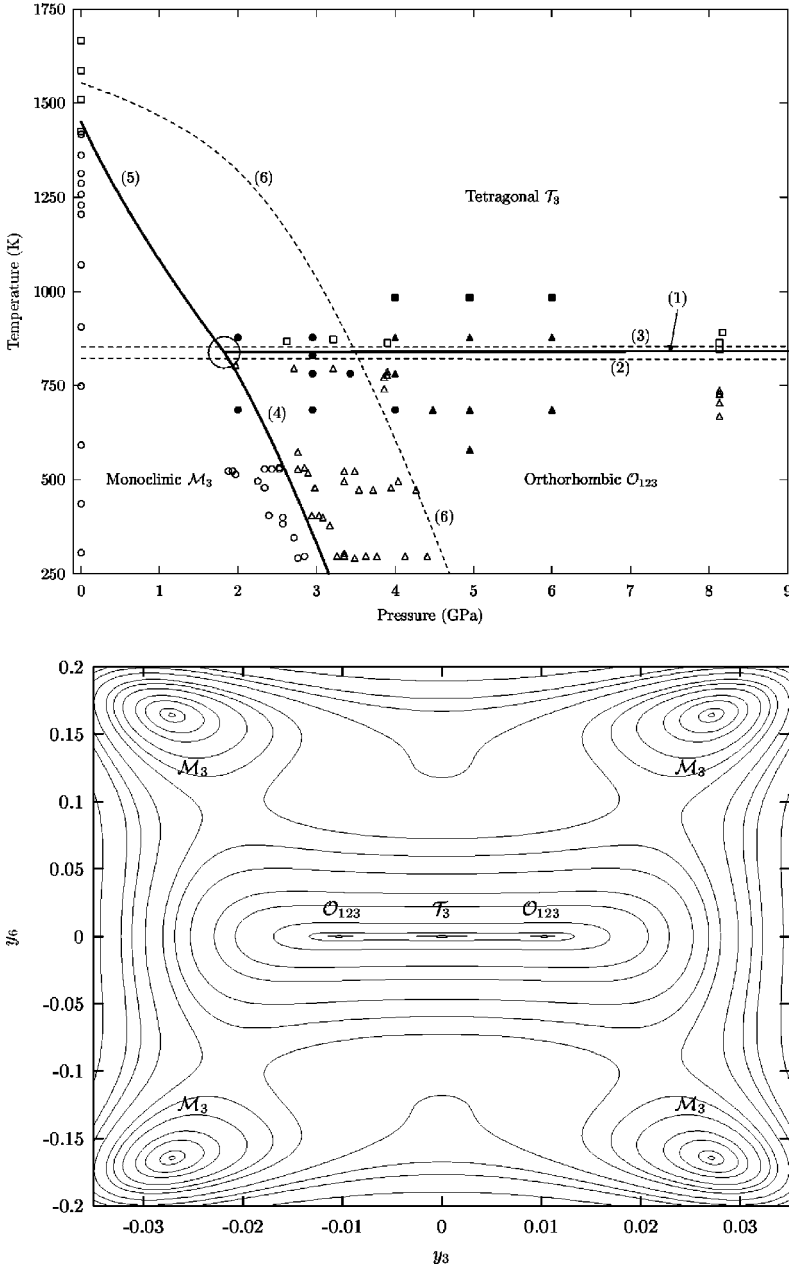
FIG. 3. Phase diagram of t-o-m zirconia in the (p,T) plane, calculated using the energy (18) with coefficients as in Eq. (19) and Tables I and II. The equilibrium phase boundaries (Maxwell lines) are the thick solid lines numbered 1, 4, and 5, which meet at the t-o-m triple point (marked by the larger circle). Indicated also are the (partially overlapping) stability domains for each of the three t-o-m phases (bounded by the dashed lines numbered 2,3,6). The circles, triangles, and squares refer to experimental observation of stable or fully transformed samples containing the m, o, and t phases, respectively. The hollow symbols at nonzero pressure refer to experiments in Ref. 16, filled symbols to data from Ref. 19, and hollow symbols at zero pressure to data from Ref. 36. The lower figure shows the level sets of the Landau potential (18) at p-T conditions near the triple point. Notice the variety of energy wells (seven) in the three-phase coexistence region.

The Landau potential ϕ_L of the system is obtained by minimizing out all the strain components other than the order parameters. We obtain

$$\phi_G = \frac{1}{2}\big[\bar{C}_{11}y_1^2 + 2\bar{C}_{12}y_1 y_2 + \bar{C}_{22}y_2^2 + (C_{11} - C_{12})y_3^2$$

$$+ C_{44}(y_4^2 + y_5^2) + C_{66}y_6^2\big] + \frac{1}{2}\big[(\bar{C}_{133}y_1 + \bar{C}_{233}y_2)y_3^2$$

$$+ (\bar{C}_{166}y_1 + \bar{C}_{266}y_2)y_6^2 + \bar{C}_{344}y_3(y_4^2 - y_5^2)\big]$$

$$+ \bar{C}_{456}y_4 y_5 y_6 + \frac{1}{4}(D_3 y_3^4 + 2L y_3^2 y_6^2 + D_6 y_6^4) + \frac{1}{6}(K_3 y_3^6$$

$$+ K_6 y_6^6) + p y_1. \qquad (15)$$

$$y_1 = \frac{1}{\Delta}\bigg[-\bar{C}_{22}p - \frac{1}{2}(H_3 y_3^2 + H_6 y_6^2)\bigg],$$

$$y_2 = \frac{1}{\Delta}\bigg[\bar{C}_{12}p - \frac{1}{2}(H_3' y_3^2 + H_6' y_6^2)\bigg],$$

$$y_4 = y_5 = 0, \qquad (16)$$

where

$$\Delta = \bar{C}_{11}\bar{C}_{22} - \bar{C}_{12}^2,$$

$$H_3 = \bar{C}_{22}\bar{C}_{133} - \bar{C}_{12}\bar{C}_{233},$$

$$H_6 = \bar{C}_{22}\bar{C}_{166} - \bar{C}_{12}\bar{C}_{266},$$

$$H_3' = \bar{C}_{11}\bar{C}_{233} - \bar{C}_{12}\bar{C}_{133},$$

$$H_6' = \bar{C}_{11}\bar{C}_{266} - \bar{C}_{12}\bar{C}_{166}. \tag{17}$$

The elimination of y_1, y_2, y_4, and y_5 leads to the following simple form of the Landau energy:

$$\phi_L = \frac{1}{2}(G_3 y_3^2 + G_6 y_6^2) + \frac{1}{4}(\tilde{D}_3 y_3^4 + 2\tilde{L} y_3^2 y_6^2 + \tilde{D}_6 y_6^4)$$

$$+ \frac{1}{6}(K_3 y_3^6 + K_6 y_6^6), \tag{18}$$

where the renormalized coefficients are given by

$$G_3 = (C_{11} - C_{12}) - \frac{H_3}{\Delta}p, \quad G_6 = C_{66} - \frac{H_6}{\Delta}p,$$

$$\tilde{D}_3 = D_3 - \frac{1}{2\Delta}(\bar{C}_{22}\bar{C}_{133}^2 - 2\bar{C}_{12}\bar{C}_{133}\bar{C}_{233} + \bar{C}_{11}\bar{C}_{233}^2),$$

$$\tilde{L} = L - \frac{1}{2\Delta}[\bar{C}_{22}\bar{C}_{133}\bar{C}_{166} - \bar{C}_{12}(\bar{C}_{133}\bar{C}_{266} + \bar{C}_{166}\bar{C}_{233})$$

$$+ \bar{C}_{11}\bar{C}_{233}\bar{C}_{266}],$$

$$\tilde{D}_6 = D_6 - \frac{1}{2\Delta}(\bar{C}_{22}\bar{C}_{166}^2 - 2\bar{C}_{12}\bar{C}_{166}\bar{C}_{266} + \bar{C}_{11}\bar{C}_{266}^2). \tag{19}$$

As is usual in Landau theory, we assume that the only tetragonal moduli that depend on temperature are $C_{11} - C_{12}$ and C_{66}, i.e., those related to the order parameters y_3 and y_6. As it is the softening of $C_{11} - C_{12}$ that triggers the $\mathcal{T}_3 \rightarrow \mathcal{O}_{123}$ transformation in Eq. (6), we set

$$C_{11} - C_{12} = A_3(T - T_0), \quad C_{66} = A_6 T + B_6. \tag{20}$$

Here $A_3 > 0$ and $A_6 \geq 0$, so that at low pressures the tetragonal phase is stable at high temperatures; in Eq. (20) T_0 is the temperature at which the t phase loses stability at zero pressure. We notice that the T dependence of C_{66} is needed in order to obtain a (p,T) dependence of the o-m transformation, as required by the phase diagram in Fig. 1.

The (p,T)-dependent values of y_3 and y_6 giving the critical points of the t-o-m Landau energy (18) are obtained by solving the equations

$$y_3(G_3 + \tilde{L}y_6^2 + \tilde{D}_3 y_3^2 + K_3 y_3^4) = 0,$$

$$y_6(G_6 + \tilde{L}y_3^2 + \tilde{D}_6 y_6^2 + K_6 y_6^4) = 0. \tag{21}$$

A simple geometric interpretation of this system and some discussion of the associated bifurcations can be found in Ref. 11.

IV. PHASE DIAGRAM, EQUILIBRIUM STRAINS, AND ELASTIC MODULI OF t-o-m ZIRCONIA

The method for fitting the coefficients appearing in the energies (15) and (18) is briefly explained in the Appendix;

TABLE I. Numerical values of the coefficients in Eqs. (15)–(18), giving the strain energy of t-o-m ZrO_2. All quantities are in GPa, except for A_3 and A_6 (in GPa K^{-1}), and T_0 (in K).

A_3	3.88×10^{-1}	A_6	2.82×10^{-3}	B_6	1.18×10^1
T_0	8.32×10^2	H_3	-5.9×10^3	H_6	-1.94×10^5
$\bar{C}_{133}$	-3×10^3	$\bar{C}_{233}$	8.17×10^3	$\bar{C}_{166}$	-6.13×10^2
$\bar{C}_{266}$	5.91	$\bar{C}_{344}$	5.61×10^1	$\bar{C}_{456}$	8.42×10^1
$\tilde{D}_3$	-9.66×10^4	$\tilde{L}$	-1.08×10^4	$\tilde{D}_6$	-2.45×10^3
K_3	6.66×10^8	K_6	7.29×10^4		

the results are given in Tables I and II. In this section we compare the computational predictions of the model with the available experimental data on ZrO_2.

A. Phase diagram

The phase diagram of t-o-m zirconia, calculated from the function ϕ_L with the coefficients taken from Tables I and II, is shown in Fig. 3. In it, we indicate the equilibrium phase boundaries (Maxwell lines), as well as the boundaries of the stability domains for the three t-o-m polymorphs. The latter are not usually indicated in the thermodynamical phase diagrams (see, for instance, Fig. 1).

The t-o-m triple point in Fig. 3 is at about 840 K and 1.8 GPa as in Ref. 16, and the three Maxwell lines, numbered 1 (t-o), 4 (o-m), and 5 (t-m), have slopes and positions in agreement with the experimental diagrams.[16,42,43] For the o-m transformation, the equilibrium pressure at room temperature is around 3 GPa (intersection of the o-m Maxwell line 4 with the p axis in Fig. 3), again in agreement with the values reported in the literature.[1,20,23] In Fig. 3 we also present various experimental observations on the transformations in different zirconia polymorphs. We notice that the monoclinic samples transform to orthorhombic symmetry in a wide area of the phase diagram, noticeably away from the o-m Maxwell line 4. This hysteresis effect almost disappears as the transformation is protracted over a number of cycles.[16]

The room-pressure value of the t-m equilibrium temperature is about 1450 K (intersection of the t-m Maxwell line 5 with the temperature axis), in agreement with Refs. 1 and 44.

TABLE II. Elastic constants and bulk modulus K of the tetragonal phase (in GPa). (a) Present model, 1500 K. (b) Estimate at 1480 K made in Ref. 52. (c) Reference 49. (d) Reference 46. (e) Reference 50. (f) Reference 4. (g) Reference 48. (h) Reference 47. The experimental values for K found in Ref. 22 are 198 and 172 GPa.

Modulus	(a)	(b)	(c)	(d)	(e)	(f)	(g)	(h)
C_{11}	307	340	416	465	327	366	395	263
C_{33}	320	325	234	326	264	286	326	262
C_{44}	100	66	39	101	59	78	105	55.9
C_{66}	16	95	73	156	64	88	56	44
C_{12}	48	33	30	83	100	180	26	15
C_{13}	209	160	68	49	62	80	42	72
K	165	183	148	173	149	180	148	122

The monoclinic equilibria in Fig. 3 are stable in the region below curve 6 (and are metastable—local energy minimizers—in the domain limited by curves 4–6). This stability range agrees well with available data on the m phase. For instance, room-pressure experiments[29,32] show that essentially all traces of monoclinic inclusions disappear above 1700 K (see the intersection of line 6 with the T axis). Also for nonzero pressure, no experimental monoclinic points are on the right of line 6 (except for a single point coming from a powdered sample).

The t-o Maxwell line number 1 is almost horizontal, with a slightly negative slope, as reported in Ref. 16; its intersection with the T axis, marking the t-o transformation temperature, is at about 840 K, in agreement with experimental data. In the vicinity of the t-o Maxwell line 1, line 2 marks the low-temperature stability boundary for the t phase, and line 3 the high-temperature existence limit for the o phase. Lines 2 and 3, which are spaced about 10-K apart, give the maximum hysteresis for the t-o transformation; this is within the experimental error given in Ref. 16. Regarding the t-o transformation, we notice that the data in Fig. 3 coming from Ref. 19 (black squares and triangles, which refer to powdered samples), would suggest a t-o Maxwell line at about 950 K, that is, more than 100-K higher than the t-o transformation temperature reported by Ref. 16. This might be due to stabilizing effects of surface layers in the microparticles used in Ref. 19.

We notice that a line marking the instability limit of the orthorhombic phase at low temperatures is absent in the calculated phase diagram, which means that, in this model, (metastable) orthorhombic energy wells are always present at the p-T conditions considered.

B. Equilibrium strains

In Fig. 4 we compare the behavior of the equilibrium strains y_1, y_2, y_3, and y_6 computed from the model with available experimental data on the m phase (no analogous data for the orthoI phase are available). The theoretical curves are obtained from the monoclinic solutions of the equilibrium equations (21) at room pressure and varying T. The experimental points indicated in Fig. 4 are derived from lattice-parameter measurements through formula (A5) in the Appendix (the parent-phase tetragonal data have been extrapolated into the range of temperatures where the monoclinic phase is stable, see Ref. 45 for an analogous procedure). As can be seen, the model reproduces well the observations, with average relative errors of 6%, 5%, 16%, and 6%, for y_1, y_2, y_3, and y_6, respectively, if compared with the strain data obtained from Refs. 35 and 36. In Fig. 4 we have also indicated the experimental points coming from Refs. 29 and 32. We notice a discrepancy between the two sets of data (especially for y_2), as well as for the temperature of complete disappearance of the m phase. The t-m transformation hysteresis is indeed known to be very sensitive to the presence of impurities in the samples.

C. Elastic moduli

The elastic moduli of the t phase enter the expression of the Gibbs potential (15) explicitly through the quadratic part
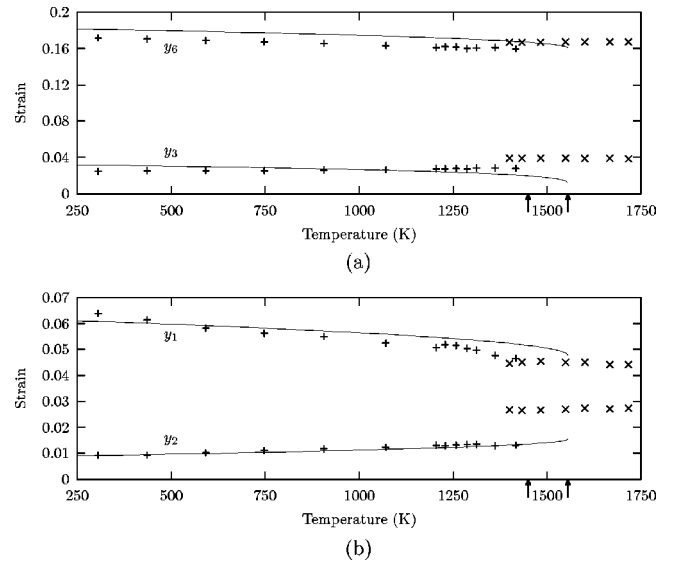

FIG. 4. The strains y_3, y_6 (a), and y_1, y_2 (b), for the monoclinic phase as functions of temperature at room pressure. Experimental points are also shown, obtained from t and m lattice-parameter data reported in Refs. 35 and 36 ($+$), and in Refs. 29 and 32 ($\times$). The computed equilibrium temperatures for the t-m transition and the stability limit of the monoclinic phase are marked by the vertical arrows; see also Fig. 3.

(11). Experimental data on these coefficients at temperatures near or above the t-m transformation and at room pressure are not available. Theoretical computations of the tetragonal moduli at various temperatures can be found in Refs. 4 and 46–49; one set of experimental values at room temperature is reported in Ref. 50 for a sample of stabilized 12 mol % Ce-doped twin-free tetragonal zirconia (see Table II).

The elastic moduli of the m phase can be computed from the model once the solutions of the equilibrium equations are known (we choose the solution with $y_3 > 0$, so that $a_m > c_m$ in the monoclinic cell). They are given by the second derivatives of the energy (15) with respect to the variables e_I (up to the relabeling of indices[51] described in Table III). The monoclinic moduli of zirconia have been investigated experimentally in some detail. Their room-pressure values at various temperatures are given in Ref. 52 [although, according to Ref. 20, "these measurements could have been perturbed by twinning, as large (homogeneous) crystals of the monoclinic phase are extremely difficult to make"]. Other data on these moduli come from the theoretical computations reported in Refs. 46 and 49—see Table IV.

As no experimental values are available for the moduli of pure tetragonal zirconia, both the tetragonal and monoclinic sets of moduli were best fitted, as described in the Appendix. The results are given in the first columns of Tables II and IV, respectively; in the same tables we also report the values of the bulk modulus K (the inverse of the coefficient of isothermal compressibility). We see that our model reproduces well the known mechanical properties of the t and m zirconia phases, except for the two monoclinic moduli C_{25}^m and C_{35}^m,

which are too high. The computed value of K in Table II is also in line with the other available estimates, and with the two experimental values (198 and 172 GPa) found, through different methods, in Ref. 22. The calculated bulk modulus for the m phase is lower than the other estimates reported in Table IV, but compares well with the value 95 GPa obtained in Ref. 20 through a Birch-Murnaghan extrapolation of *in situ* measurements.

Finally, the elastic moduli of the *o* phase can also be evaluated from the model; however, no direct experimental data are available for a check. The bulk modulus of the *o* phase computed from our energy is 165 GPa, which compares satisfactorily with the estimate of 205 GPa obtained in Ref. 20, through a Birch-Murnaghan interpolation of experimental data.

V. CONCLUSIONS

The sixth-order polynomial energy presented here provides a coherent description for the tetragonal, orthoI, and monoclinic phases of zirconia and the associated transformations below 1700 K and 8 GPa, and in the strain range indicated in the lower part of Fig. 3. The equilibrium strains, elastic moduli, and p-T phase diagram (including quantitative estimates of the stability domains for each phase) calculated from the model are in good agreement with the available experimental data. Further data on these ZrO_2 polymorphs, in particular for the orthoI phase, can be estimated from, or fitted into, the present framework. Important information that may be assessed by means of our energy includes, for instance, the reaction of the material to shear loads; in particular, various phase diagrams involving nonhydrostatic loading variables can be established. This should lead to a better understanding of the behavior of the zirconia inclusions within a ceramic matrix.[14]

Figure 5 shows the bifurcations for the equilibria in our model, at room pressure and varying temperature (the energy coefficients are taken from Table I). In this diagram we observe the complex topology of the connections among the branches of stable and unstable equilibria; in particular, we notice that in addition to the three branches corresponding to the t-o-m phases observed around the triple point of Figs. 1 and 3, there is also an "extra" branch of stable orthorhombic solutions with $y_3 = 0$ and $y_6 \neq 0$. These orthorhombic equilibria have the following point group:

TABLE III. Correspondence between the conventional indexing of the monoclinic moduli (based on a twofold axis along the b direction) and the second derivatives of the Gibbs potential in Eqs. (10)–(15).

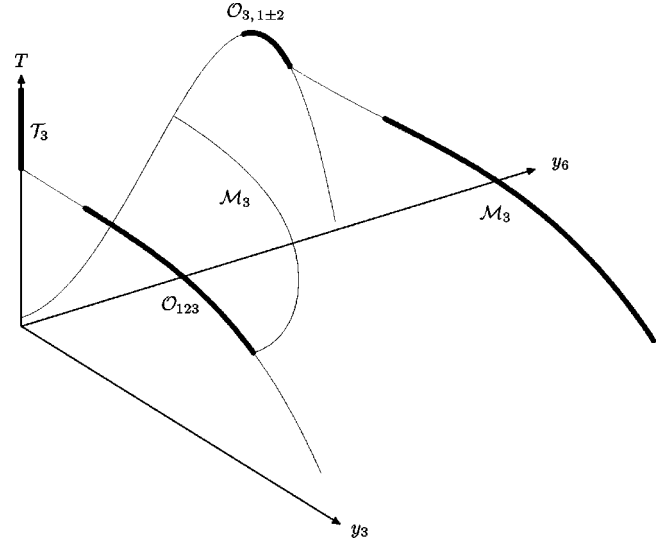| C_{IJ}^m	$\partial^2 \phi_G / \partial e_R \partial e_S$	C_{IJ}^m	$\partial^2 \phi_G / \partial e_R \partial e_S$	C_{IJ}^m	$\partial^2 \phi_G / \partial e_R \partial e_S$
11	22	12	23	13	12
15	26	22	33	23	13
25	36	33	11	35	16
44	55	46	45	55	66
66	44				

FIG. 5. Bifurcation diagram for the critical points of the Landau energy (18), at room pressure and varying temperature T (thick and thin lines indicate stable and unstable equilibria, respectively). The bifurcations are all subcritical. In order to show the connections between the branches, T is made to vary in an unphysical range. For clarity, only the branches with $y_3 \geq 0$ and $y_6 \geq 0$ are shown; the pattern is extended by symmetry to the entire (y_3, y_6) plane.

$$\mathcal{O}_{3,1\pm2} = \{1, R_{t_3}^\pi, R_{t_1+t_2}^\pi, R_{t_1-t_2}^\pi\}, \tag{22}$$

which should be compared with Eq. (3). The existence of such an extra phase appears as a necessary consequence of our unified Landau description of t-o-m zirconia. One can check that near $p = 0$ the $\mathcal{O}_{3,1\pm2}$ wells exist only in a small range of temperatures (above 1520 K), and that these equilibria are unstable for p above 1.35 GPa. Furthermore, the new orthorhombic minimizers always have relatively high energy, and are surrounded by lower barriers than the other

TABLE IV. Elastic constants and bulk modulus K of the monoclinic phase (in GPa). (a) Present model, 1500 K. (b) Reference 52, 1273 K. (c) Reference 46. (d) Reference 49. The experimental value for K obtained in Ref. 20 is 95 GPa.

Modulus	(a)	(b)	(c)	(d)
C_{11}^m	356	350	353	347
C_{22}^m	320	341	434	364
C_{33}^m	274	312	272	274
C_{44}^m	99	81.6	156	88
C_{55}^m	145	66.3	123	108
C_{66}^m	101	101	192	122
C_{12}^m	281	171	233	164
C_{13}^m	40	35.2	138	102
C_{15}^m	56	4.3	61	28
C_{23}^m	137	155	191	156
C_{25}^m	102	9.4	−44	−17
C_{35}^m	146	3.2	59	11
C_{46}^m	−14	−13.9	−35	−44
K	84	180	182	194

t-o-m wells. However, one may speculate that the $\mathcal{O}_{3,1\pm2}$ phase might gain more stability and physical relevance at nonhydrostatic loading conditions.

APPENDIX

The computation of the coefficients of the Gibbs energy was done in two steps. First, we estimated the values of the coefficients through the procedure outlined below. Then, an extensive search was performed in the neighborhood of such values in order to achieve an overall best fit of the moduli, transition temperatures and pressures, and equilibrium strains.

We start by evaluating the equilibrium strains, which are necessary in many of the ensuing computations. These are found through lattice-parameter interpolations. For the t phase we use the experimental data from Ref. 35 and the compressibilities reported in Ref. 22. This gives the following values of the lattice parameters in nanometers (with T in K and p in GPa):

$$a_t = 0.5056(1 + 1.254 \times 10^{-5}T)(1 - 1.41 \times 10^{-3}p),$$

$$c_t = 0.5167(1 + 1.459 \times 10^{-5}T)(1 - 2.24 \times 10^{-3}p).$$
(A1)

The above expressions are also used to extrapolate a_t into the range of temperatures where the other phases are stable [see Eqs. (A3) and (A5) below]. To compute the strains of the orthorhombic equilibria, we take the t-o orientation relationship (2) given by Ref. 1, and account for the cell doubling occurring along $[100]_o$. The strain tensor is then

$$E = \frac{1}{2}\begin{pmatrix} \left(\dfrac{c_o}{a_t}\right)^2 - 1 & 0 & 0 \\ 0 & \left(\dfrac{a_o}{2a_t}\right)^2 - 1 & 0 \\ 0 & 0 & \left(\dfrac{b_o}{c_t}\right)^2 - 1 \end{pmatrix}, \quad (A2)$$

so that

$$y_{3,o} = \frac{1}{2\sqrt{2}}\left[\left(\frac{c_o}{a_t}\right)^2 - \left(\frac{a_o}{2a_t}\right)^2\right], \quad (A3)$$

with a_t as above. The lattice parameters for the orthorhombic phase are (in nanometers)

$$a_o = 1.0137(1 + 2.72 \times 10^{-6}T)(1 - 1.24 \times 10^{-3}p),$$

$$b_o = 0.5308(1 + 1.18 \times 10^{-6}T)(1 - 1.60 \times 10^{-3}p),$$

$$c_o = 0.5141(1 + 6.04 \times 10^{-6}T)(1 - 2.49 \times 10^{-3}p).$$

These are linear interpolations of the *in situ* measurements reported in Refs. 20 and 53 for the compressibilities, and in Ref. 18 for the thermal expansion. The t-m orientation relationships are assumed to be as in Eq. (4), which give the following strain tensor for the monoclinic equilibria:

$$E = \frac{1}{2}\begin{pmatrix} \left(\dfrac{c_m}{a_t}\right)^2 - 1 & \dfrac{2a_m c_m \cos\beta_m}{a_t^2} & 0 \\ \dfrac{2a_m c_m \cos\beta_m}{a_t^2} & \left(\dfrac{a_m}{a_t}\right)^2 - 1 & 0 \\ 0 & 0 & \left(\dfrac{b_m}{c_t}\right)^2 - 1 \end{pmatrix}.$$
(A4)

By Eq. (10) the strains y_I of the monoclinic phase are then

$$y_{3,m} = \frac{1}{2\sqrt{2}}\left[\left(\frac{c_m}{a_t}\right)^2 - \left(\frac{a_m}{2a_t}\right)^2\right],$$

$$y_{6,m} = \frac{a_m c_m \cos\beta_m}{a_t^2}, \quad (A5)$$

with the following monoclinic lattice parameters (in nanometers and rads):

$$a_m = 0.51248(1 + 9.7172 \times 10^{-6}T)(1 - 2.92 \times 10^{-3}p),$$

$$b_m = 0.52019(1 + 1.6800 \times 10^{-6}T)(1 - 2.97 \times 10^{-4}p),$$

$$c_m = 0.52883(1 + 1.4138 \times 10^{-5}T)(1 - 2.20 \times 10^{-3}p),$$

$$\beta_m = 1.73677(1 - 5.9905 \times 10^{-6}T)(1 - 2.72 \times 10^{-4}p).$$
(A6)

These interpolations are found by fitting the experimental data from Ref. 36, with compressibilities as in Refs. 1, 20, 22, and 54.

By using Eqs. (19) and (20) and the fact that the tetragonal solutions lose stability for $G_3 = 0$, we can compute A_3 and T_0, using the elastic moduli of the t phase (taken here from Ref. 47). By interpreting the experiments reported in Ref. 16 as indicating the temperature at which the t phase loses stability, we obtain the virtual t-o transformation temperature at room pressure to be $T_0 = 832 \pm 24$ K;[55] Eq. (20) gives then $A_3 = 0.388$ GPa K^{-1}.

The latent heat of the transformation between the t and m phases, occurring at $T_{trs} = 1478$ K, $p_{trs} = 0$, has been measured[44,56] to be $Q = \Delta H_{trs} = -5.941$ kJ mol^{-1} (from t to m). Then the entropy jump ΔS_{trs} can be estimated from

$$\Delta S_{trs} = \frac{\Delta H_{trs}}{T_{trs}} = -\frac{1}{2}(A_3 y_3^2 + A_6 y_6^2); \qquad (A7)$$

the values of the strains y_3 and y_6 needed in Eq. (A7) are taken from Eq. (A5). We obtain $\Delta S_{trs} = -4.02$ J mol^{-1} K^{-1}; by using the molar volume of the reference tetragonal state at the same temperature, we convert the entropy into J m^{-3} K^{-1}, which gives for A_6 and B_6 the values 2.82×10^{-3} GPa K^{-1} and 11.8 GPa, respectively. Notice that A_6 is very small, meaning that the temperature dependence of C_{66} is practically negligible.

In our model the three lines characterizing the transition between the o and t phases (lines 1, 2, and 3, in Fig. 3) have the same slope, and their equations are, respectively,

$$G_3 = \frac{3\tilde{D}_3^2}{16 A_3 K_3}, \quad G_3 = 0, \quad G_3 = \frac{\tilde{D}_3^2}{4 K_3},$$

or, in (p, T) coordinates [see Eqs. (19) and (20)],

$$T = T_0 + \frac{3\tilde{D}_3^2}{16 A_3 K_3} + \frac{H_3}{A_3 \Delta} p, \quad T = T_0 + \frac{H_3}{A_3 \Delta} p,$$

$$T = T_0 + \frac{\tilde{D}_3^2}{4 A_3 K_3} + \frac{H_3}{A_3 \Delta} p.$$

According to Ref. 16 the slope of the o-t equilibrium phase boundary is -0.29 K GPa^{-1}, with a large standard deviation of 2.7 K GPa^{-1} due to reported experimental difficulties. This gives $H_3/\Delta = -0.112$, and $H_3 = -5.9 \times 10^3$ GPa. To obtain H_6, we use Eq. (16) at zero pressure; by Eq. (10), the

monoclinic strain y_1 is calculated as the trace of the strain matrix in Eq. (A4). Given the above value of H_3, we obtain $H_6 = -1.94 \times 10^5$ GPa.

The remaining coefficients of the Landau energy are determined from the set of equations defining the triple point. For the m phase and the t-m Maxwell line one has three conditions: two are the equilibrium equations (21), yielding the values of the order parameters y_3 and y_6, and the third one is the equality of the Landau energies for the t and m phases. Similar conditions hold for the o equilibria and the t-o Maxwell line. The triple point is fixed at about $p = 1.8$ GPa and $T = 840$ K, which roughly corresponds to the average of the two values given in Ref. 16 (obtained in the conditions of increasing and decreasing temperatures and pressures). The numerical solution of the corresponding system of equations is

$$\tilde{D}_3 = -1.16 \times 10^5 \text{ GPa}, \quad \tilde{D}_6 = -6.41 \times 10^3 \text{ GPa},$$

$$\tilde{L} = -1.29 \times 10^4 \text{ GPa},$$

$$K_3 = 7.93 \times 10^8 \text{ GPa}, \quad K_6 = 1.84 \times 10^5 \text{ GPa}.$$

Finally, four of the third-order moduli appearing in ϕ_G come from Eq. (17), in which the values of H_3 and H_6 are as above, while H_3' and H_6' are determined from Eq. (16) with the use of two experimental values for y_2 at different temperatures. This gives the values of $\bar{C}_{133}$, $\bar{C}_{233}$, $\bar{C}_{166}$, and $\bar{C}_{266}$; $\bar{C}_{344}$ and $\bar{C}_{456}$ are in turn obtained by adjusting the values of the monoclinic elastic moduli C_{46}^m and C_{66}^m (see Table IV).

---

*Electronic address: fadda@dmsa.unipd.it

†Electronic address: trusk@aem.umn.edu

‡Electronic address: zanzotto@dmsa.unipd.it

[1] *Zirconia Engineering Ceramics*, edited by E. H. Kisi (Trans. Tech., Ütikon-Zürich, 1998).

[2] It is likely that the atomic degrees of freedom within the cell and their coupling with strain play a role in the t-o-m transformations of zirconia. However, since the atomic movements within the lattice cell of t-o-m zirconia are very complex, and as there is virtually no information about them, only the strain parameters have been considered here. This is not too reductive, as our main aim is to produce a phenomenological model at the macroscopic level. A discussion of the motif's role in the energetics of some zirconia phases can be found in Refs. 3–5. Our strain energy can, in principle, be obtained through the adiabatic elimination of the internal variables from the more general potentials that couple strains and atomic motions, as was proposed by Born in his molecular theory of elasticity, see Refs. 6–8.

[3] K. Negita and H. Takao, J. Phys. Chem. Solids **50**, 325 (1989).

[4] S. Fabris, A. T. Paxton, and M. W. Finnis, Phys. Rev. B **61**, 6617 (2000).

[5] Y. Ishibashi and V. Dvořak, J. Phys. Soc. Jpn. **58**, 4211 (1989).

[6] M. Born, *Dynamik der Kristallgitter* (Tuebner, Leipzig, 1915).

[7] M. Born and K. Huang, *Dynamical Theory of Crystal Lattices* (Clarendon Press, Oxford, 1954).

[8] I. Stakgold, Quarterly J. Math. **8**, 169 (1950).

[9] J. L. Ericksen, Arch. Ration. Mech. Anal. **73**, 99 (1980).

[10] J. L. Ericksen, Int. J. Solids Struct. **22**, 951 (1986).

[11] L. Truskinovsky and G. Zanzotto, J. Mech. Phys. Solids **50**, 189 (2002).

[12] B. Budiansky and L. Truskinovsky, J. Mech. Phys. Solids **41**, 1445 (1993).

[13] N. Simha and L. Truskinovsky, in *Contemporary Research on the Mechanics and Mathematics of Materials*, edited by R. C. Batra and M. F. Beatty (CIMNE, Barcelona, 1996).

[14] N. Simha and L. Truskinovsky, Acta Mater. **42**, 3827 (1994).

[15] S. K. Chan, Physica B **150**, 212 (1988).

[16] S. Block, J. A. H. da Jornada, and G. J. Piermarini, J. Am. Ceram. Soc. **68**, 497 (1985).

[17] E. H. Kisi, C. J. Howard, and R. J. Hill, J. Am. Ceram. Soc. **72**, 1757 (1989).

[18] C. J. Howard, E. H. Kisi, R. B. Roberts, and R. J. Hill, J. Am. Ceram. Soc. **73**, 2828 (1990).

[19] O. Ohtaka, T. Yamanaka, S. Kume, E. Ito, and A. Navrotsky, J. Am. Ceram. Soc. **74**, 505 (1991).

[20] J. M. Léger, P. E. Tomaszewski, A. Atouf, and A. S. Pereira, Phys. Rev. B **47**, 14 075 (1993).

[21] J. K. Dewhurst and J. E. Lowther, Phys. Rev. B **57**, 741 (1998).

[22] P. Bouvier, E. Djurado, G. Lucazeau, and T. Le Bihan, Phys. Rev. B **62**, 8731 (2000).

[23] O. Ohtaka, H. Fukui, T. Kunisada, T. Fujisawa, K. Funakoshi, W. Utsumi, T. Irifune, K. Kuroda, and T. Kikegawa, Phys. Rev. B **63**, 174108 (2001).

[24] The zirconia structure with orthorhombic symmetry considered here is called "orthoI."[20,21] The respective space groups of the t-o-m phases in our model are $P4_2/nmc$ ($Z=2$), $Pbca$ ($Z=8$, brookite-type structure), and $P2_1/c$ ($Z=4$, baddeleyite-type structure); here Z denotes the number of chemical formulas per primitive unit cell. At higher pressures and temperatures zirconia also crystallizes in a number of other structures, some of which have been only partially investigated, see the diagram in Fig. 1 and Refs. 20–23.

[25] Our primitive tetragonal skeletal cell contains four ZrO_2 units ($Z=4$), and has twice the volume of the actual unit cell of the primitive tetragonal zirconia crystal.

[26] M. Pitteri and G. Zanzotto, *Continuum Models for Phase Transitions and Twinning in Crystals* (Chapman and Hall, London, 2002).

[27] R. N. Patil and E. C. Subbarao, Acta Crystallogr., Sect. A: Cryst. Phys., Diffr., Theor. Gen. Crystallogr. **26**, 535 (1970).

[28] E. C. Subbarao, H. S. Maiti, and K. K. Srivastava, Phys. Status Solidi A **21**, 9 (1974).

[29] H. Boysen, F. Frey, and T. Vogt, Acta Crystallogr., Sect. B: Struct. Sci. **47**, 881 (1991).

[30] G. K. Bansal and A. H. Heuer, Acta Metall. **22**, 409 (1974).

[31] We recall that the t-m orientation relationships $c_t \| a_m$, and $c_t \| c_m$, have also been reported in the literature (Refs. 30, and 32–34). These are produced by deformations generating monoclinic lattices whose point groups are the monoclinic subgroups $\mathcal{M}_{1+2}$ and $\mathcal{M}_{1-2}$ in Eq. (8), leading to the t-m path indicated in Eq. (7). Therefore, we cannot completely exclude that the mechanism (7) plays a role in the t-m phase change of ZrO_2.

[32] F. Frey, H. Boysen, and T. Vogt, Acta Crystallogr., Sect. B: Struct. Sci. **46**, 724 (1990).

[33] G. R. Hugo and B. C. Muddle, Mater. Sci. Forum **56-58**, 357 (1990).

[34] N. K. Simha, J. Mech. Phys. Solids **45**, 261 (1997).

[35] S. M. Lang, J. Am. Ceram. Soc. **47**, 641 (1964).

[36] R. N. Patil and E. C. Subbarao, J. Appl. Crystallogr. **2**, 281 (1969).

[37] If y_6 is applied to a $\mathcal{T}_3$-tetragonal lattice it produces a base-centered orthorhombic structure whose point group is the orthorhombic subgroup $\mathcal{O}_{3,1\pm2}$ of $\mathcal{T}_3$ appearing in formula (22) of Sec. V. The strains $y_4 = e_4$ and $y_5 = e_5$ are similar to y_6, but act in the (100) and (010) tetragonal planes, respectively. They produce monoclinic lattices with point groups as in Eq. (8), which are irrelevant for the transformation mechanism (6). See Ref. 26 for full details on symmetry breaking in simple lattices.

[38] L. D. Landau and E. M. Lifshits, *Theory of Elasticity* (Pergamon Press, Oxford, 1986).

[39] M. E. Gurtin, *An Introduction to Continuum Mechanics* (Academic Press, New York, 1981).

[40] J. K. Liakos and G. A. Saunders, Philos. Mag. A **46**, 217 (1982).

[41] *Elastic, Piezoelectric, and Related Constants of Crystals*, edited by R. F. S. Hearmon, Landolt-Börnstein, New Series, Group III, Vol. 11 (Springer-Verlag, Berlin, 1984).

[42] G. L. Kulcinski, J. Am. Ceram. Soc. **51**, 582 (1968).

[43] *Phase Diagrams for Zirconium and Zirconia Systems*, edited by H. M. Ondik and H. F. McMurdie (National Institute of Standards and Technology/American Ceramic Society, Columbus, OH, 1998).

[44] M. W. Chase, *NIST-JANAF Thermochemical Tables*, 4th ed., Number 9, in J. Phys. Chem. Ref. Data Monogr. (National Institute of Standards and Technology, Gaithersburg, MD, 1998).

[45] M. A. Carpenter, E. K. H. Salje, A. Graeme-Barber, B. Wruck, M. T. Dove, and K. S. Knight, Am. Mineral. **83**, 2 (1998).

[46] R. E. Cohen, M. J. Mehl, and L. L. Boyer, Physica B **150**, 1 (1988).

[47] S. K. Chan (private communication), see Ref. 50.

[48] A. P. Mirgorodsky, M. B. Smirnov, and P. E. Quintard, Phys. Rev. B **55**, 19 (1997).

[49] A. P. Mirgorodsky and P. E. Quintard, J. Am. Ceram. Soc. **82**, 3121 (1999).

[50] E. H. Kisi and C. J. Howard, J. Am. Ceram. Soc. **81**, 1682 (1998).

[51] In order to compare the moduli computed from our model to those obtained experimentally for the m phase, one must relabel them as in Table III. This is because, according to the transformation mechanism (6), the twofold axis in the monoclinic crystal derives from the tetragonal fourfold axis, which is labeled the c axis, as is standard for the tetragonal system; thus in our monoclinic phase the twofold axis is not the b axis conventionally used for the monoclinic system, but is, instead, the c axis.

[52] S. Chan, Y. Fang, M. Grinsditch, Z. Li, M. V. Nevitt, W. M. Robertson, and E. S. Zouboulis, J. Am. Ceram. Soc. **74**, 1742 (1991).

[53] O. Ohtaka, T. Yamanaka, S. Kume, N. Hara, H. Asana, and F. Izumi, Proc. Jpn. Acad., Ser. B: Phys. Biol. Sci. **66**, 193 (1990).

[54] N. M. Balzaretti and J. A. H. da Jornada, Phys. Rev. B **52**, 9266 (1995).

[55] We say "virtual" because, as is seen in experimental phase diagrams (see, for instance, Refs. 16, 42, and 43) and in Fig. 3, this transition actually does not occur at pressures below 2 GPa; thus T_0 is obtained by continuing line (2) in Fig. 3 to its intersection with the $p=0$ axis.

[56] J. P. Coughlin and E. G. King, J. Am. Chem. Soc. **72**, 2262 (1950).